Defence Technology 22 (2023) 88–98

Contents lists available at ScienceDirect

Defence Technology

journal homepage: www.keaipublishing.com/en/journals/defence-technology

The role of physical properties in explosive welding of copper to stainless steel

G.H.S.F.L. Carvalho [a, b, *], I. Galvão [a, c], R. Mendes [d], R.M. Leal [a, e], A.B. Moreira [f], A. Loureiro [a]

[a] Univ Coimbra, CEMMPRE, Departamento de Engenharia Mecânica, Rua Luís Reis Santos, 3030-788, Coimbra, Portugal
[b] Department of Industrial Engineering, University of Firenze, Via di Santa Marta 3, 50139, Firenze, Italy
[c] ISEL, Departamento de Engenharia Mecânica, Instituto Politécnico de Lisboa, Rua Conselheiro Emídio Navarro 1, 1959-007, Lisboa, Portugal
[d] Univ Coimbra, ADAI, LEDAP, Departamento de Engenharia Mecânica, Rua Luís Reis Santos, 3030-788, Coimbra, Portugal
[e] LIDA-ESAD.CR, Instituto Politécnico de Leiria, Rua Isidoro Inácio Alves de Carvalho, 2500-321, Caldas da Rainha, Portugal
[f] Univ. Porto, LAETA/INEGI, Dept. Eng. Metalúrgica e de Materiais, R. Dr. Roberto Frias, 4200-465, Porto, Portugal

ARTICLE INFO

Article history:
Received 6 June 2022
Received in revised form
4 August 2022
Accepted 18 August 2022
Available online 5 September 2022

Keywords:
Explosive welding
Solid-state
Copper-stainless steel
Dissimilar
Interface morphology
Weldability

ABSTRACT

This paper investigates the effects of the physical properties on the microstructure and weldability of explosive welding by joining two metals with a significant contrast in thermophysical properties: stainless steel and copper. Sound welds between stainless steel and copper were obtained, and the interfacial morphology was wavy, regardless of the position of the materials. The weldability of dissimilar pairs was found to be more dependent on the relationship between the physical properties of the base materials than on the absolute value of the material property. When there is a significant difference in thermal conductivity between the flyer and the base plate, together with a material with a low melting temperature, the weldability of the pair is often poor. The relative position of the plates affects the interfacial microstructure even when similar morphologies are found. For the metallic pairs studied, the wave size was bigger for the configuration in which the ratio between the density of the flyer and the density of the base plate is smaller. The same phenomenon was observed for the impedance: bigger waves were found for a smaller ratio between the impedance of the flyer and the impedance of the base plate.

1. Introduction

Dissimilar joining between metallic alloys is a strategic tool for manufacturing components that need a combination of properties that cannot be found in a single alloy. There are many ways to achieve a consistent joint between alloys, such as connectors, adhesive bonding, and welding. Welding presents some advantages, but it may be very difficult or even impossible to achieve by the traditional fusion welding processes when welding materials with extreme differences in physical properties, especially the melting temperature. For this type of welding, it is necessary to use non-conventional technologies, such as solid-state processes. The explosive welding (EXW) process is one of the most interesting solid-state processes for welding dissimilar materials with significantly different physical properties because bulk melting is not required. EXW results in reduced heat-affected zones and maintains the mechanical properties of the original material after the welding process. Thus, it has an excellent potential for the manufacture of claddings, a process of great importance in several sectors, including defence [1–3], aerospace [4,5], oil & gas [6], and chemical [7].

The two main elements in EXW are the flyer and the base plate. The flyer plate is the projected plate, i.e. the plate that is driven by the energetic material and moves towards the base plate. In turn, the base plate is positioned below the flyer at rest and receives the impact of the flyer. In general, some authors indicate that the flyer has a greater influence on the process [8,9], which is often verified by the difficulty in welding some materials, especially when positioned as a flyer [10]. For dissimilar welding, this is relevant because, besides each property alone, the combination of properties of each material should be analysed.

* Corresponding author. Univ Coimbra, CEMMPRE, Departamento de Engenharia Mecânica, Rua Luís Reis Santos, 3030-788, Coimbra, Portugal.
E-mail address: gustavo.carvalho@unifi.it (G.H.S.F.L. Carvalho).
Peer review under responsibility of China Ordnance Society

https://doi.org/10.1016/j.dt.2022.08.016

It is known that welding metallic pairs with significantly different physical properties is possible but can be problematic in explosive welding. Many welding combinations represent today a great industrial and academic relevance, such as the welding of aluminium and carbon steel [11–15], aluminium and copper [14,16–18], aluminium and stainless steel [10,12–14,19,20], copper and stainless steel [21–23]; stainless steel and carbon steel [24], aluminium and titanium [25,26], aluminium and magnesium [27], titanium and steel [28–30], titanium and stainless steel [31,32]; titanium and copper [33], and less common but relevant alloys such as welding using niobium [19,34,35], tantalum [31, 34, 36–38], tungsten [39,40] and zirconium [41]. Recently, some investigations have also been focused on process advances, successfully developing strategies to reinforce the mechanical properties of the joints [20,42,43].

Among these pairs, the copper-stainless steel combination is of high scientific and industrial importance. These alloys present very particular features, such as resistance to corrosion, thermal and electrical conductivity (copper), and good ductility at low temperatures. These properties, if combined, would generate a unique component. However, these two alloys are extremely different regarding some of their physical properties, such as the thermal conductivity (copper has a thermal conductivity of 398 W/(m·K) and AISI 304 stainless steel has a thermal conductivity of 16.2 W/(m·K)) and, to a lesser extent, the melting temperature (copper melts at 1085 °C and the AISI 304 stainless steel melts at 1400 °C approximately).

Differences in thermal conductivity may hinder welding and represent an important topic of research. In a previous work [10], the problem of welding materials with significantly different thermal conductivities was addressed by studying the welding between aluminium and stainless steel by EXW. The difficulty of joining this pair by EXW became evident and it was analysed how to maximise/increase the chances of achieving a good-quality weld between them. However, copper and stainless steel present an even more notable dissimilarity in thermal conductivity, and different metallurgical transformations. It is necessary to address topics relating to process development to increase the body of knowledge regarding dissimilar welding of materials with different physical properties.

The objective of the present work is to analyse the phenomena of the explosive welding process by welding materials with significant contrasts in thermophysical properties, in this case, stainless steel to copper. The work will discuss the effect of the physical properties on explosive welding comprehensively, investigating aspects like weldability and interfacial/wave morphology. The research was performed using optical microscopy, scanning electron microscopy (SEM) with energy-dispersive X-ray spectroscopy (EDS), electron backscattering diffraction (EBSD), tensile-shear mechanical testing, and microhardness measurements.

2. Materials and methods

Two series of welds between copper and stainless steel were performed using explosive welding in a parallel full overlap joint configuration similar to Loureiro et al. [14]. For both weld series, the welded plates had a width of 70 mm, length of 250 mm, and a thickness of 3 mm. The copper plate was a Cu-DHP alloy (94 HV0.2), and the stainless steel was an austenitic AISI 304 alloy (188 HV0.2). Two arrangements were tested: the copper as the flyer plate and the stainless steel as the base plate (Cu/SS), and one with the stainless steel as the flyer plate and the copper as the base plate (SS/Cu). Table 1 shows the identification and the main welding parameters used for both welding series. The energetic mixture used was ANFO.

Table 1
Welding conditions.

Welding conditions	Weld series	
	Cu/SS	SS/Cu
Flyer plate alloy	Cu-DHP	AISI 304
Base plate alloy	AISI 304	Cu-DHP
Stand-off distance (mm)	4.5	4.5
Explosive Mixture	ANFO	ANFO
Explosive Ratio	1	1

The detonation velocity (v_d) was measured in all tests according to the procedure adopted by Mendes et al. [24,44]. Samples were removed longitudinally to the detonation propagation (welding direction) and prepared for metallographic analysis. The samples were examined using a Leica DM4000 M LED optical microscope and a Zeiss Merlin VP Compact scanning electron microscope equipped with EDS. The deformation and grain structure of the weld interface was analysed by EBSD through an FEI Quanta 400FEG ESEM/EDAX Genesis X4M microscope equipped with OIM Analysis software.

The mechanical integrity of the welds was analysed by tensile-shear testing and microhardness. Localised microhardness measurements (HV0.025 and HV0.01) were performed using an HMV-G Shimadzu tester at the weld interface. The tensile-shear tests were executed in quasi-static loading conditions (1 mm/min), using a 100 kN universal testing machine, Shimadzu AGS-X. Three specimens (removed longitudinally), designed similarly to that reported by Carvalho et al. [12,13,19], were tested for both weld series. This type of test was chosen due to the type of application for which the component will be used, as well as to ensure comparison with previous results. Similar specimens are found in standards, such as in ASTM D3165, and previous works [19,45]. The strain fields of the specimens were acquired by digital image correlation (DIC) using a GOM Aramis 5 M system. The methodology to prepare the specimens to process/analyse the strain data is detailed in Leitão et al. [46]. The fracture surfaces obtained during the tests were evaluated by SEM.

3. Results and discussion

3.1. Welding results and weldability analysis

Table 2 presents the values measured for the detonation velocity (v_d) (which is the same as the collision point velocity (v_c) for parallel welding configuration) and the values computed for the impact velocity (v_p). The impact velocity was calculated using Gurney's equation for a one-dimensional problem in parallel configuration (Eq. (1)) [47,48]. Despite being widely accepted, this equation presents some limitations. It ignores the acceleration of the flyer plate and hence represents only the terminal velocity [47,49]. Thus, the proximity of the value calculated with Gurney's equation and the real one depends on the STD chosen.

Table 2
Values of detonation/collision point velocity, impact velocity and welding results.

Weld series	v_d, v_c (m/s)	v_{pF} (m/s)	Welding results
Cu/SS	2420	446	consistent joint
SS/Cu	2186	403	consistent joint

$$v_{p_F} = \sqrt{2E}\left(\frac{3R^2}{R^2+5R+4}\right)^{\frac{1}{2}} \quad (1)$$

where R is the explosive ratio and $\sqrt{2E}$ is the Gurney characteristic velocity of the explosive (m/s). An empirical correlation presented by Cooper [50] for ideal explosives ($\sqrt{2E} = V/2.97$) was used to estimate this parameter. Some of the limitations of this approach have been reported by Carvalho et al. [51]. An alternative process to determine this parameter was presented by Mendes et al. [24].

There are different methods to establish the weldability window. Ribeiro et al. [52] discussed the weldability window concept, reviewing the main equations used for its calculation. In the present work, for the calculation of the minimum impact pressure (represented by the lower limit), the equation based on Deribas and Zakharenko's work [53] was used (Eq. (2)). In all equations, the letters "f" and "b" (subscripts) indicate whether the property refers to the flyer or base plate, respectively).

$$\beta = k\sqrt{\frac{H_H}{\rho_{fb}\cdot v_C^2}} \quad (2)$$

where k is a constant related to the cleanliness and roughness of the surface, H_H is the hardness of the hardest material (Pa), ρ_{fb} is the average density between the flyer and base plate (kg/m^3), and v_C is the collision point velocity (m/s).

The upper limit of the window represents the maximum kinetic energy permissible to avoid excessive melting. Carpenter and Wittman [54] formulate an equation to represent this phenomenon (Eq. (3)) in their work.

$$v_P = \frac{1}{N}\frac{\left(T_{mf}\cdot C_{Bf}\right)^{1/2}}{v_c}\frac{\left(\lambda_f\cdot c_f\cdot C_{Bf}\right)^{1/4}}{\left(\rho_f\cdot\delta_f\right)^{1/4}} \quad (3)$$

where N is a constant, T_m is the melting temperature (°C), C_B is the bulk sound velocity (m/s), λ is the thermal conductivity (W/(m·K)), c is the specific heat (J/(kg·K)), ρ is the density (kg/m^3), δ is the thickness (m), and v_C is the collision point velocity (m/s). The constant N was used according to Rosset's work [55].

The limit on the left refers to the minimum velocity to obtain a wavy interface. This limit is not critical since the presence of waves is not imperative for the welding to occur [48]. This limit was calculated using Cowan's equation [56] in Eq. (4).

$$R_T = \frac{\left(\rho_f+\rho_b\right)\cdot v_C^2}{2\cdot\left(H_f+H_b\right)} \quad (4)$$

where R_T is the critical Reynolds number, ρ is the density (kg/m^3), v_C is the collision point velocity (m/s), and H is the hardness (Pa).

The limit on the right represents the jet formation, essential for a consistent weld. This limit is usually not a concern because the welding is often performed at lower velocities. So, this limit was simplified to the bulk sound velocity in the flyer plate. Loureiro et al. [14] explained this simplification in more detail.

Fig. 1 shows the weldability windows calculated for each welding series. The blue area represents the Cu/SS weldability window, while the red area represents the weldability window of the SS/Cu weld series. According to the weldability window theory, the Cu/SS weld series has a better theoretical weldability because it presents a broader area of suitable welding parameters to achieve a consistent weld. The blue circle and the red triangle represent the location of the welds performed in the weldability windows according to their welding parameters.

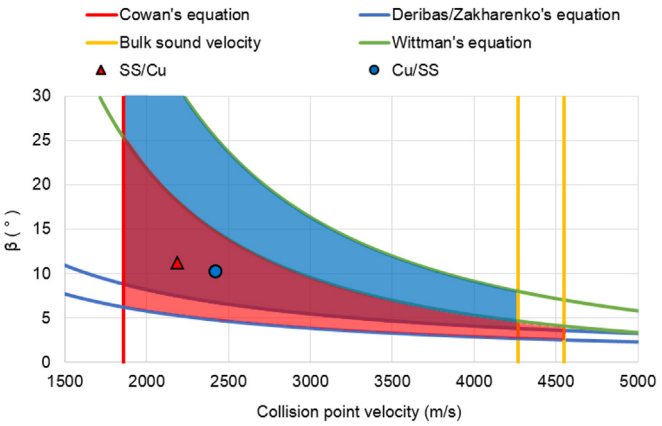

Fig. 1. Weldability windows. The blue area represents the Cu/SS window, and the red area represents the SS/Cu weld series.

The welding of stainless steel and copper is very relevant for the study of the explosive welding process. Stainless steel and copper have notable differences in some of their physical properties, which explain the importance of studying this combination when compared to other dissimilar combinations. A pertinent combination to compare with the present work is the welding of aluminium and stainless steel (Al-SS) because of its particularities, especially the differences in thermal conductivity of the materials. By analysing the present experiments and comparing them to other studies about welding aluminium and stainless steel, it is possible to affirm that welding copper and stainless steel is easier than welding aluminium and stainless steel. The welding of copper to stainless steel was consistent for both configurations (Cu/SS and SS/Cu), presenting good bonding characteristics. On the other hand, Al-SS welding is problematic when stainless steel is used as the flyer plate [10].

In a previous work concerning Al-SS welding [10], the authors addressed the issue of the low thermal conductivity of the flyer plate (stainless steel) compared to the base plate (aluminium). However, as the authors state, the differences in properties should be analysed individually for each specific combination of materials. Regarding copper to stainless steel, the differences in thermal conductivity between the alloys are more significant than in Al-SS welding. However, when analysing the weldability window and the experiments, this noticeable difference in thermal conductivity did not represent an issue. Besides the thermal conductivity, the differences in melting temperature and density between the aluminium alloy and the stainless steel must be taken into consideration regarding the low weldability in Al-SS welding. The weldability is good when welding aluminium to aluminium [51,57,58], despite the low density and melting temperature because there is no difference in these properties between the flyer and base plate. So, analysing the Al–Al, Al-SS and Cu-SS welds together, only the Al-SS combination proved to have very low weldability. As the present work shows that Cu-SS has good weldability, the weldability issue of the Al-SS combination is not caused only by the difference in thermal conductivity.

In an Al–Al similar weld, both materials have a low density and melting temperature, but the welding is easy because the plates have the same properties. So, the heat flux and heat at the interface are distributed more uniformly. The weld does not have a significant preferential heat flow or accumulation in some locations on the interface, which could be caused by differences in the physical

Table 3
Analysis of the physical properties [61] compared to the weldability.

	Thermal conductivity (W/(m·K))		Melting temperature °C		Experimental weldability
	flyer	base	flyer	base	
Al-Al [51]	247	247	660	660	Good
Cu-Fe [62,63]	398	80	1085	1538	Good
Fe-Cu [64,65]	80	398	1538	1085	Good
Cu-SS (present work)	398	16.2	1085	1400	Good
SS-Cu (present work)	16.2	398	1400	1085	Good
Cu-Al [16,51,66]	398	247	1085	660	Good
Al-Fe [12]	247	80	660	1538	Good/Average
Fe-Al [11]	80	247	1538	660	Average
Al-Cu [17,66]	247	398	660	1085	Average
Al-SS [10,12]	247	16.2	660	1400	Average/Poor
SS-Al [10]	16.2	247	1400	660	Poor

properties of the flyer and base plate.

Carpenter and Wittman [54] stated that the thermal conductivity of the flyer is related to the dissipation of heat at the interface to avoid excessive melting. That said, welding materials with significant thermal conductivity differences will influence how the heat will be distributed at the interface. The thermal conductivity gradient for the Al-SS combination may cause a preferential heat flux that leads to an accumulation of heat on the aluminium plate, which has a very low melting temperature. Furthermore, the presence of Fe_xAl_y intermetallic compounds at the interface intensifies this problem because they increase the interface's solidification time (and solidification range) during welding, which decreases the weldability [11]. When these issues are acting concurrently, it may significantly hinder the welding process. The fact that the intermetallic phases present in Al–Fe combinations are aluminium-rich [11,59,60] also supports this theory.

Thus, comparing Cu-SS welding to Al-SS welding, and despite the notable difference in thermal conductivities between copper and stainless steel, the melting temperature of the copper is not as low as that of aluminium. Moreover, Fe and Cu do not form intermetallics under equilibrium, which increases the overall weldability of the pair and results in better weldability than the Al-SS pair.

Table 3 shows the melting temperature, thermal conductivity, and the experimental weldability of many metallic combinations. The data shows that when there is a significant difference in thermal conductivity between the flyer and the base plate, together with a material with a low melting temperature, the weldability is poor. Especially when the material with a low melting temperature is positioned as the flyer plate and the most conductive material has a very low melting temperature, the heat will accumulate on this material and favour an excessive melting. In other words, the results suggest that when there is an uneven distribution of heat and one of the materials being welded has a low melting temperature, the welding is difficult.

3.2. Morphological analysis of the interface

The morphology of the interface of explosive welded joints is one of the weld's most essential characteristics. Depending on the alloys being welded, unetched samples are valuable to analyse the morphological and geometrical aspects of the interface and the presence of defects. Fig. 2 and Fig. 3 show the analysis by optical microscopy using unetched samples. The images show a difference in wave size between the two series of welds, both for wavelength and height. Using stainless steel as the flyer (SS/Cu), the waves present a greater wavelength and height. The Cu/SS presented an average wavelength of 430 μm and a height of 157 μm, while the SS/Cu series presented an average wavelength of 646 μm and a height of 274 μm. The SS/Cu series presented a wavelength and height of 50% and 75% bigger, respectively.

It is known that the wavelength and height/amplitude increase when the explosive ratio [25, 67–70], the stand-off distance [70,71], and impact velocity increase [12]. However, the welds have the same stand-off distance and explosive ratio; and the impact velocity is lower for the weld with the biggest wavelength and height. This suggests that, in this case, the difference in wavelength and height is due to the positioning of the plates and not to the welding parameters.

Prümmer [72] studied the wavelength and height/amplitude of the interfacial waves of explosive welded joints. The author shows that the usual equation for estimating these characteristics uses mainly geometrical aspects such as the thickness of the plate and the collision angle (which depends on the explosive ratio). However, the author suggests that, in order to estimate the wavelength and amplitude more accurately, it is essential to consider the properties of the materials as well. The fact that the experimental results in the present work show a variation in wavelength and height/amplitude using the same thicknesses of the plates and the same ratio (consequently the same collision angle considering the welding configuration) agrees with the theory proposed by Prümmer [72].

Experimental studies to test the effects of each physical property are not straightforward in explosive welding because there are many process parameters and many phenomena occurring simultaneously. The resulting interface in explosive welding is influenced by several interconnected aspects, which makes its analysis very important. In addition to the welding parameters, the physical properties are of great importance because they influence almost every aspect of obtaining a certain interface morphology and weld quality. The density will directly influence the resulting kinetic energy [73,74], the thermal conductivity will influence the temperature distribution [54,75,76], and melting temperature will influence the deformation, presence of melting and formation of intermetallic phases at the interface [54,75–77]. These interconnected factors synergistically influence the energy transferred to the process, the deformation, heat transfer, metallurgical interaction and consequently the weld's final morphology and overall quality [56,78,79]. One way to analyse these effects is to relate the physical properties to experimental observation to investigate any trend in the results that may be related to a property. Many metallic pairs and their tendency to have bigger or smaller waves have been observed to do this type of analysis. Table 4 shows some metallic pairs with results from the literature for alternative positioning configurations (changing the positioning between the flyer and base plate). The alloy that appears first on the identification is the flyer plate (“Cu/SS”, for instance, indicates that the copper alloy is the flyer, and the SS is the base plate). The table includes some physical properties of the flyer (identified as F), the base plate (identified as B) and the ratio between them (identified as R, meaning the flyer property/base plate property). The objective is to identify the properties that may influence the occurrence of smaller or bigger waves depending on the positioning of the plates. Analysing the interface of welds of the same materials under different positions allows us to evaluate the influence of the properties with regard to the positioning. If a trend in the wave morphology related to the same properties for multiple metallic pairs is observed, it may help to understand the properties that may instigate the increase in the size of the waves.

By analysing the ratio of the properties in Table 4, it is possible to identify a tendency in the results related to the density and impedance. According to Grady's interpretation [80], in a simplified way, the impedance of a material can be defined as the velocity at

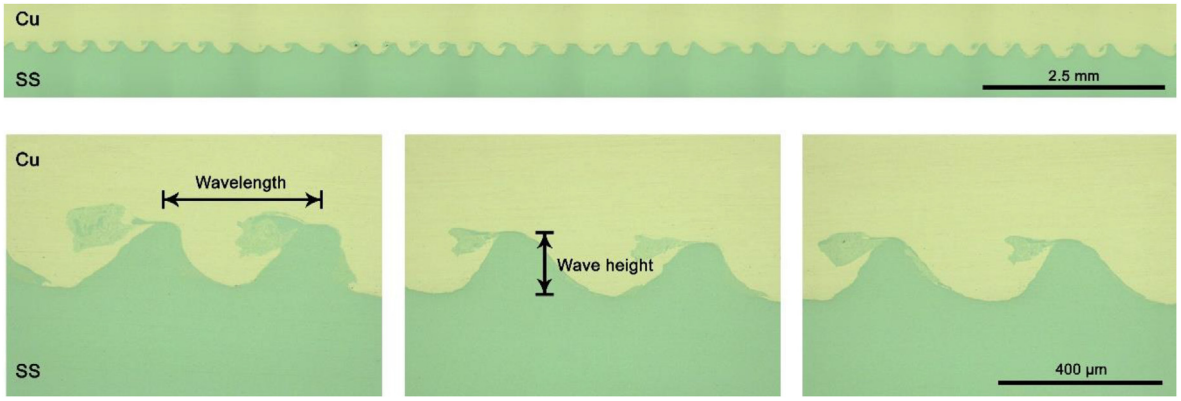

Fig. 2. Unetched microstructure of the Cu/SS weld.

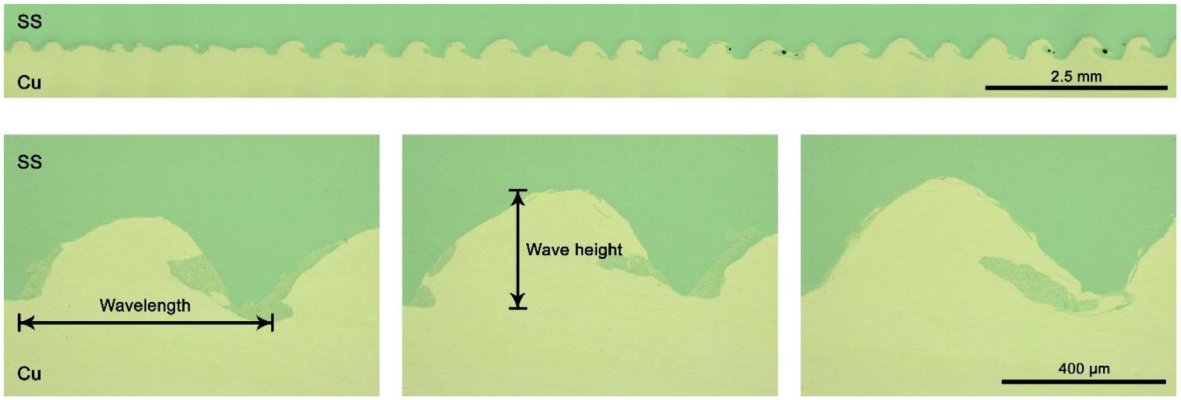

Fig. 3. Unetched microstructure of the SS/Cu weld.

Table 4
Ratio of some physical properties of metallic pairs.

		Pair 1		Pair 2		Pair 3		Pair 4		Pair 5	
		Cu/SS	SS/Cu	Cu/Al [51,66]	Al/Cu [17]	Fe/Al [11]	Al/Fe [12]	Ta/Al [31]	Al/Ta [36]	SS/Ti [31]	Ti/SS [32]
Melting Temperature (°C)	F	1085	1400	1085	660	1538	660	3017	660	1400	1668
	B	1400	1085	660	1085	660	1538	660	3017	1668	1400
	R	0.78	1.29	1.64	0.61	2.33	0.43	4.57	0.22	0.84	1.19
Thermal Conductivity	F	398	16.2	398	247	80	247	54.4	247	16.2	11.4
(W/(m·K))	B	16.2	398	247	398	247	80	247	54.4	11.4	16.2
	R	24.57	0.04	1.61	0.62	0.32	3.09	0.22	4.54	1.42	0.70
Density (g/cm^3)	F	8.96	8	8.96	2.7	7.87	2.7	16.4	2.7	8	4.5
	B	8	8.96	2.7	8.96	2.7	7.87	2.7	16.4	4.5	8
	R	1.12	0.89	3.32	0.30	2.91	0.34	6.07	0.16	1.78	0.56
Impedance	F	38.3	36.4	38.3	14.5	36.5	14.5	55.6	14.5	36.4	22
(kg/(m^2·s) × 10^6)	B	36.4	38.3	14.5	38.3	14.5	36.5	14.5	55.6	22	36.4
	R	1.05	0.95	2.64	0.38	2.52	0.40	3.83	0.26	1.65	0.60
Wave size		Smaller	Bigger	Smaller*	Bigger	Smaller*	Bigger	Smaller*	Bigger	Smaller	Bigger

Where the identifications F, B and R in the second column indicate whether the property belongs to the flyer (F), the base plate (B) or the ratio between them, i.e. the flyer property/base plate property (R). "*" identifies welds without waves or with an essentially flat interface.

which the propagating wave subsumes the mass of the body. For all the metallic pairs, when the ratios of the density and impedance are higher, the wave size is smaller. On the copper-stainless steel combination, the copper alloy possesses the highest density and impedance. So, when positioned as the flyer, the size of the waves is smaller than when positioned as the base plate. The same tendency occurs for all the other metallic pairs. The facts observed from these studies must be cautiously analysed because they are independent experiments, so there may be differences in some of the experimental conditions and methods used.

This fact is crucial because it agrees with the issue raised by Prümmer [72] decades ago that is the size of the waves is not affected only by the welding parameters and geometrical aspects (such as collision angle and thickness of the plates). Many investigations in the last few decades have addressed the effect of geometrical characteristics and welding parameters [25,67–70]. However, no work details the effects of physical properties. Although the physical phenomenon that explains this tendency is unclear, this trend has been identified for all these pairs.

Despite these differences in wavelength and amplitude, the

morphology type of the interface is the same (wavy) regardless of the positioning of the SS and Cu plates. This happens because the physical properties that significantly influence the morphology are not extremely different between the plates. Carvalho et al. [51] discuss these properties in more detail, addressing the wave interface factor (WIF), which is influenced by the density and melting temperature. The interfaces that were found agree with the WIF theory [51].

Another noteworthy characteristic found during the microstructural analysis is that independently of the position of the plates (i.e. regardless of the positioning of the copper or stainless steel plate), the wave is formed by the copper with the steel material inside it (in vortexes) – Figs. 2 and 3. Carvalho et al. [19] analysed the types of waves in many dissimilar EXW welds and suggested that the material forming the wave is always the material with the higher density and shock impedance. Many studies confirm this theory [12,17,68,81,82]. The present results agree with this theory because the copper alloy possesses a higher density and impedance than the stainless steel. This behaviour has been detected for many different metallic combinations such as Al–Mg, Al–Cu, Al–Nb, Al–Fe, Cu–W, Ta-SS, Ti–Cu, Ti–Fe, Ti-SS, Zr-Fe [19]. The same study [19] introduces the impedance mismatch factor (IMF), another morphological theory for EXW, which addresses the type of waves in dissimilar welds: curled or typical. Despite both combinations in the present work presenting an IMF for typical waves, it is close to the threshold and the waves are slightly more curled and less symmetrical. Table 5 shows the results for the WIF and IMF. It indicates that the expected interface is wavy, with typical waves, in agreement with the experimental results.

The three features studied (type of morphology, type of waves and size of the waves) represent some of the most critical aspects of the interface. It is noteworthy that these three characteristics seem to be related to density, impedance and melting temperature. In particular, the density (and indirectly the impedance, since it depends on the density) is related to those three aspects. The study by Cowan et al. [56], one of the most important studies regarding the morphology of the interface, also addresses the density and includes the hardness. With that being said, it is possible that a more general and broad equation analysing all these properties and relating all these studies could be developed.

3.3. Microstructural analysis

Fig. 4 and Fig. 5 present the SEM images of both weld series. It is possible to detect some plastic deformation, especially for the copper alloy, there are also vortex regions next to the waves (arrows). The welding between the copper and stainless steel represents the interaction mainly of iron, copper and chromium. It is essential to highlight that the Fe–Cu equilibrium diagram does not foresee the formation of intermetallic compounds [83]. Additionally, under equilibrium, chromium (which is the second most present element after Fe in the SS alloy - approximately 18% in weight) also does not form intermetallic phases with copper [83]. Regarding the interaction of chromium and iron, the sigma intermetallic phase may precipitate, but this transformation is much less likely in EXW.

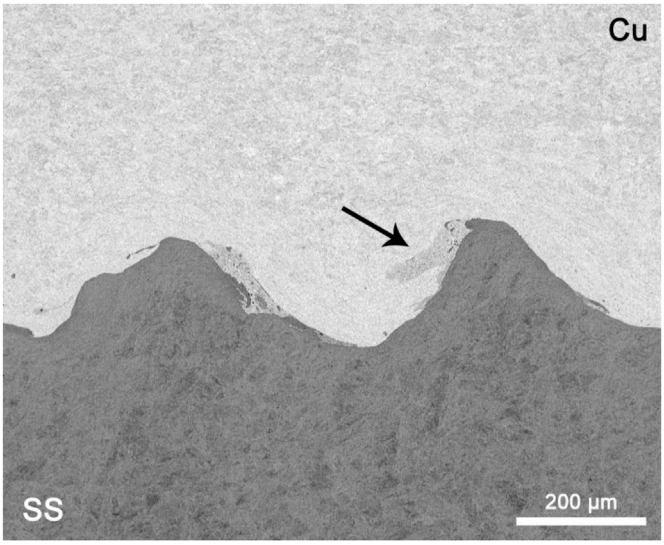

Fig. 4. SEM analysis of the Cu/SS weld series.

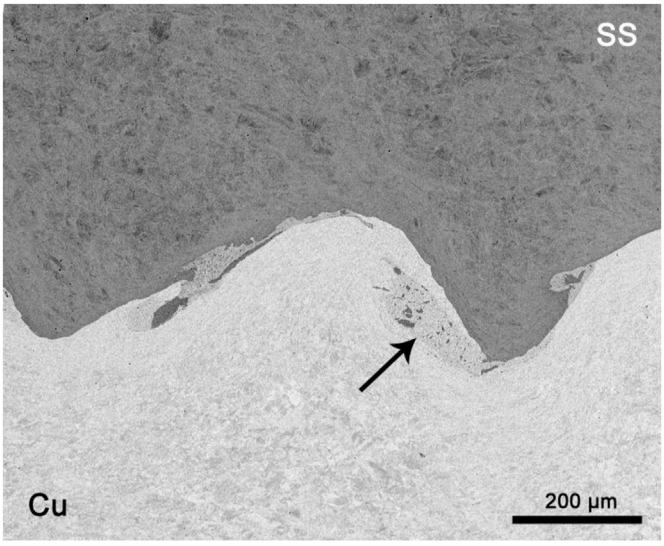

Fig. 5. SEM analysis of the SS/Cu weld series.

It should be noted that EXW is a welding process that occurs under extreme conditions that may lead to transformations outside the equilibrium represented by the phase diagrams. So, non-equilibrium phases may form. However, both Fe–Cu and Cr–Cu combinations do not form intermetallic phases under equilibrium (a fact supported by their phase diagrams), suggesting that

Table 5
Calculation of the WIF and IMF.

	WIF theory [51] >5.1 the interface is flat <4.2 the interface is wavy		IMF theory [19] >0.31 the wave is curled <0.21 the wave is typical		
	WIF value [51]	Expected morphology	IMF value [19]	Expected type of waves	Result
Cu-SS	0.87	Wavy	0.052	Typical	Typical waves (Fig. 2)
SS-Cu	1.15	Wavy	0.050	Typical	Typical waves (Fig. 3)

intermetallic formation is unlikely. EDS and EBSD analysis combined with microhardness measurements were done at these vortex regions to verify this fact.

Table 6 shows the results of the EDS analysis and the microhardness at the interface. The Cu/SS weld series presented a range of 158–237 HV at mixed regions at the interface, while the SS/Cu weld series presented a range of 140–213 HV. The samples also presented some measurements with a significant increase in hardness in the stainless steel due to the plastic deformation/work hardening next to the interface, typical for the EXW process. Fig. 6 and Fig. 7 show some of the microhardness measurements. The EDS semi-quantitative chemical analysis confirms it is a mixed region. The microhardness is higher than the hardness of the base materials before welding, but as showed in previous works, both the copper [16,51] and the stainless steel [10,13] present a significant increase in hardness after the impact. That said, the values obtained at the interface range between the hardness of copper and stainless steel after welding. So, the measurements do not suggest the formation of a brittle intermetallic compound and no cracks were observed. Using the EBSD technique, the presence of intermetallic phases was also not detected. Therefore, none of the results obtained indicates the presence of brittle intermetallic phases at the interface. Fig. 8 and Fig. 9 show the locations of the EDS analyses.

An EBSD analysis was performed to complement the microstructural analysis. Fig. 10 and Fig. 11 present the inverse pole Fig. (IPF) maps, indicating intense deformation at the interface. The deformation in explosive welding is important to promote good metallurgical bonding between the materials, and a wavy interface is reported to be the most favourable interfacial morphology.

In both welds, it is possible to identify the formation of waves, the presence of elongated plastically deformed grains, and grain refinement in regions close to the interface line (Figs. 10 and 11). The phenomenon of grain refining has already been identified in other works [38,77,84,85]. Some authors [38,65] explain that this grain refinement at the interface is due to significant plastic deformation caused by the severe conditions of the explosive welding process, such as high pressure and its singular thermal cycle. Regardless of the position in the weld, the elongated grains are present in greater quantity on the copper side of the interface, while on the stainless steel side, there is a more significant presence of refined grains. The two weld series did not present significant differences between them.

The microstructure and morphology of the weld interface are crucial in EXW, as they are the result of the combination of all factors and phenomena of the welding process. The results show that physical properties play a fundamental role in the process, as they influence the thermal, mechanical, and metallurgical conditions experienced at the weld interface. This analysis becomes more complex in the case of dissimilar joining because metallurgical compatibility issues must also be considered in addition to all the phenomena already inherent to the process. Moreover, each material has its physical and mechanical properties, and to separate the individual contribution of each material, i.e. to separate the individual contribution of the flyer plate and the base plate, is extremely difficult.

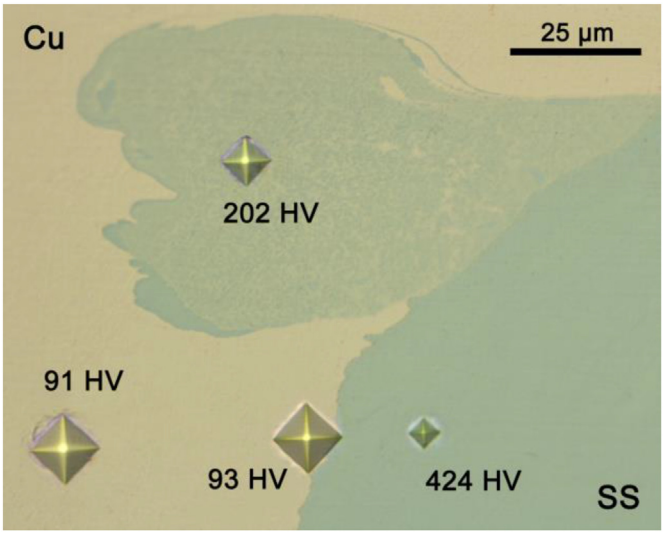

Fig. 6. Microhardness measurements at the interface of the Cu/SS weld (HV0.01).

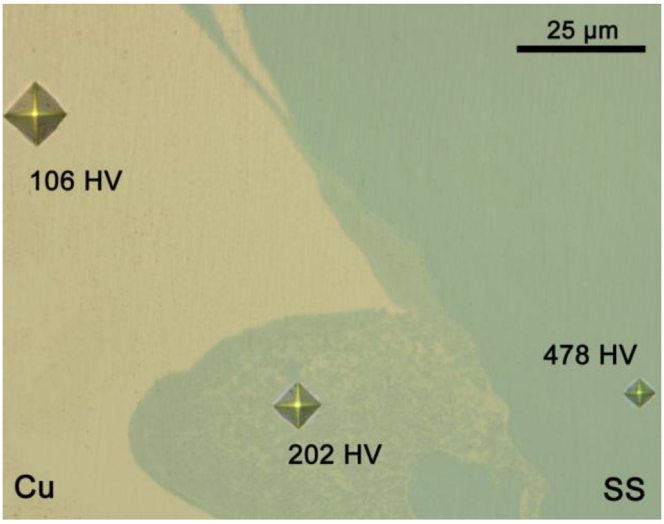

Fig. 7. Microhardness measurements at the interface of the SS/Cu weld (HV0.01).

3.4. Mechanical integrity

Table 7 shows the results of the tensile-shear tests. The weld series presented similar results concerning the strength of the joints and the behaviour of the fracture. All tests fractured outside the weld, always in the copper plate (the flyer in the Cu/SS weld and the base plate in the SS/Cu weld). Linse and Temple [86] indicate that excessively large waves may be detrimental because the small pockets of jet material located on their front and back slopes (see the arrows in Figs. 4 and 5) would be larger. So, with larger melted

Table 6
Properties of the mixed region.

Weld	Figure	Zone	Chemical composition (atomic %)					Microhardness range at the interface
			Cu	Fe	Cr	Ni	Si	
Cu/SS	Fig. 8	A	4.40	68.90	17.54	7.74	1.42	158–237 HV0.025
		B	73.17	18.78	5.45	2.60	–	
SS/Cu	Fig. 9	C	88.76	7.35	2.14	1.75	–	140–213 HV0.025
		D	3.64	69.60	18.04	7.76	0.96	

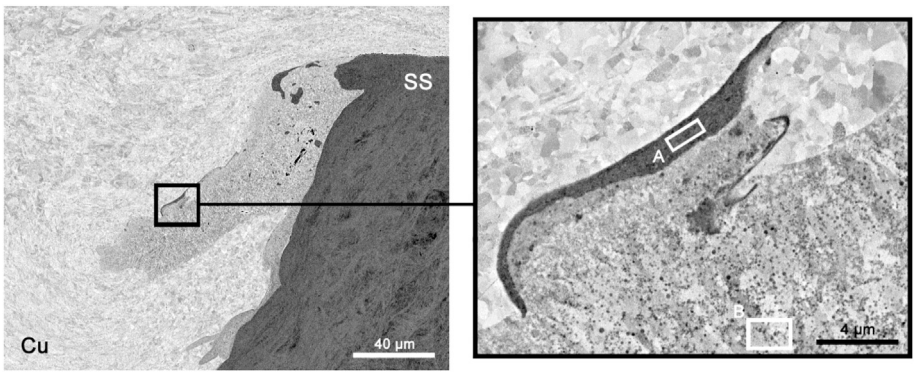

Fig. 8. SEM images of the Cu/SS weld.

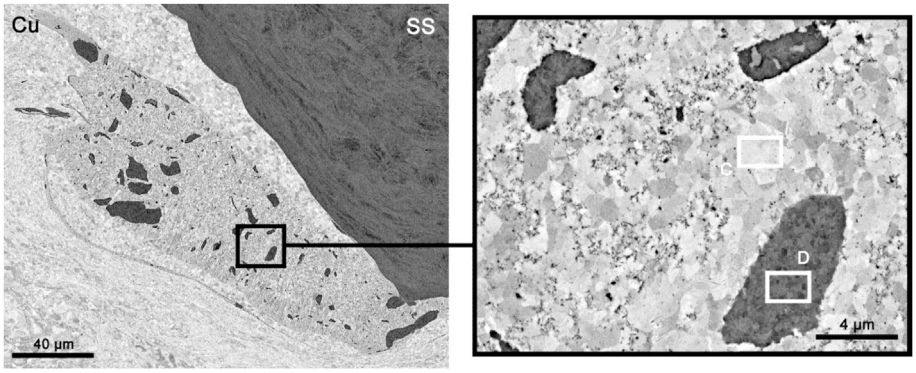

Fig. 9. SEM images of the SS/Cu weld.

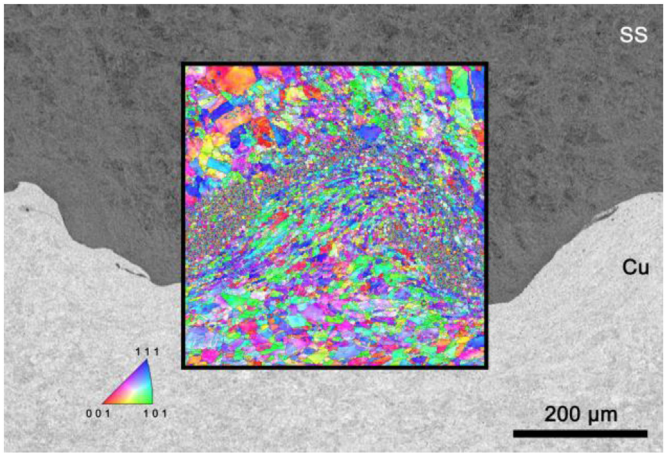

Fig. 10. Inverse pole Fig. map from the EBSD analysis of the Cu/SS weld. For comparison purposes, the image was rotated (stainless steel is facing upwards).

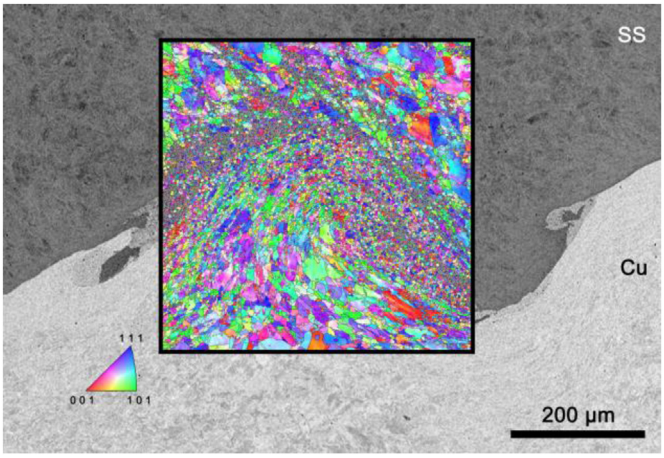

Fig. 11. Inverse pole Fig. map from the EBSD analysis of the SS/Cu weld.

zones, a higher number of shrinkage voids, small cracks and other discontinuities that reduce strength and ductility may be present [38]. However, despite the differences in wave size between the Cu/SS and SS/Cu welds, all specimens from both series fractured outside the weld region in the tensile-shear tests. Therefore, the results suggest that the wave size and the weld interface's morphological characteristics are not related to the difference in mechanical properties. It is also worth noting that the difference in mechanical properties is not large.

Fig. 12 and Fig. 13 show the DIC pictures at the maximum load and a picture after the fracture. As reported above, the fractures occurred in the copper alloy, and the deformation is also concentrated in the same alloy. This happens due to the low strength of the copper alloy compared to the stainless steel. The SEM fracture analysis indicates that both welds presented ductile fractures, with the typical dimples. Fig. 14 shows the aspect of the fracture of the Cu/SS weld series. The fractures were analysed, and a 100% ductile fracture surface was found for all samples. As Carvalho et al. [12] stated, favourable interfacial morphologies may improve the mechanical performance of the weld. As Figs. 2 and 3 show, a regular wavy interface was found for both weld series. Further, the absence

Table 7
Results of the tensile-shear tests.

Weld	Range of Maximum loads (kN)	Fracture region	Fracture mode
Cu/SS	12.7 to 13.6	Outside the weld (copper flyer plate)	Ductile
SS/Cu	12.3 to 13.1	Outside the weld (copper base plate)	Ductile

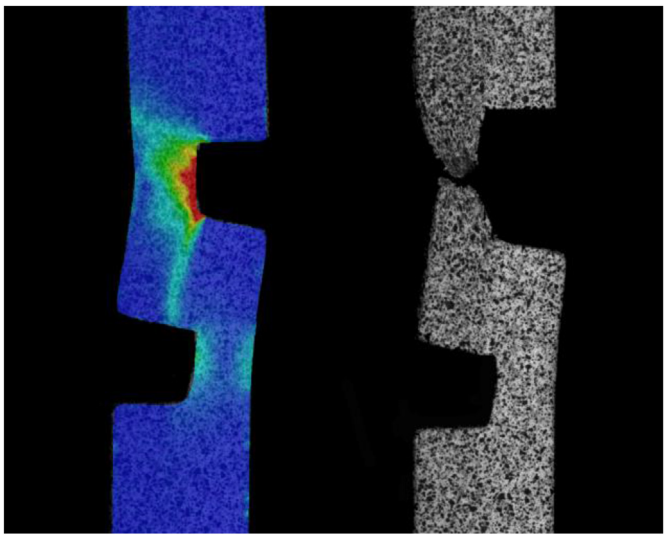

Fig. 12. DIC of the Cu/SS weld.

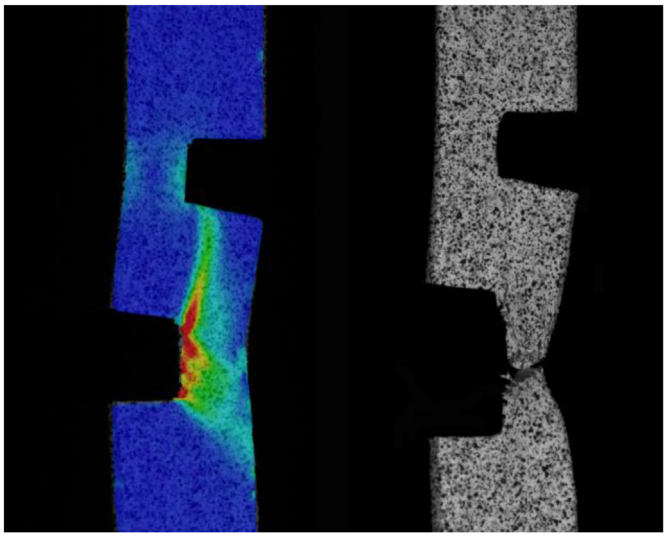

Fig. 13. DIC of the SS/Cu weld.

of brittle IMCs is a positive fact regarding the overall ductility of the joint. The combination of the absence of IMCs and, especially, a favourable interface resulted in a very good mechanical performance.

4. Conclusions

The aim of the present work was to analyse the phenomena of the explosive welding process through the dissimilar welding of two materials with a significant contrast in thermophysical properties: stainless steel and copper. The following conclusions were drawn:

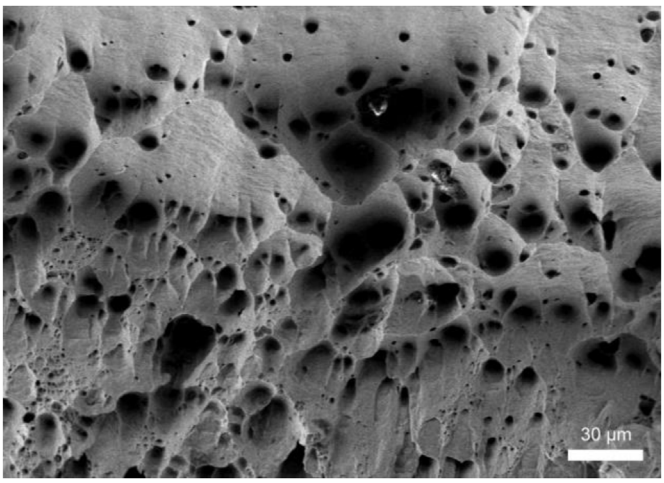

Fig. 14. SEM analysis of the fracture surface of the Cu/SS weld. Both weld series presented the same fracture mechanism.

(1) Sound Cu/SS and SS/Cu welds with excellent mechanical behaviour can be achieved using an ANFO-based explosive mixture. The non-formation of intermetallic phases at the weld interface has a positive effect on the weldability of this welding pair;
(2) The weldability of dissimilar pairs was found to be strongly influenced by the physical properties of the materials, but it is more dependent on the mismatch of the materials properties being welded than on the value of the properties itself. When there is a significant difference in thermal conductivity between the flyer and the base plate, together with a low melting temperature material, the weldability of that pair of materials is often poor;
(3) The relative position of the plates has some influence on the weld interface even when similar morphologies are found. The interfacial waves of the SS/Cu welds have a higher height/amplitude and wavelength than those of the Cu/SS welds;
(4) For the metallic pairs studied, the wave size was found to be bigger for the configuration in which the ratio between the density of the flyer and the density of the base plate is smaller. The same phenomenon was observed for the shock impedance: bigger waves were found for a smaller ratio between the impedance of the flyer and the impedance of the base plate.

Declaration of competing interest

The authors declare that they have no known competing financial interests or personal relationships that could have appeared to influence the work reported in this paper.

Acknowledgements

This research is sponsored by FEDER funds through the program COMPETE – Programa Operacional Factores de Competitividade –

and by national funds through FCT – Fundação para a Ciência e a Tecnologia, under the project UIDB/00285/2020.

References

[1] Mahesh V, Joladarashi S, Kulkarni SM. Damage mechanics and energy absorption capabilities of natural fiber reinforced elastomeric based bio composite for sacrificial structural applications. Def. Technol. 2021;17:161–76. https://doi.org/10.1016/j.dt.2020.02.013.

[2] Luo F, Cockburn A, Sparkes M, Lupoi R, Chen Z, O'Neill W, et al. Performance characterization of Ni60-WC coating on steel processed with supersonic laser deposition. Def. Technol. 2015;11:35–47. https://doi.org/10.1016/j.dt.2014.09.003.

[3] Crouch IG. Body armour – new materials, new systems. Def. Technol. 2019;15:241–53. https://doi.org/10.1016/j.dt.2019.02.002.

[4] Xie MX, Zhang LJ, Zhang GF, Zhang JX, Bi ZY, Li PC. Microstructure and mechanical properties of CP-Ti/X65 bimetallic sheets fabricated by explosive welding and hot rolling. Mater Des 2015;87:181–97. https://doi.org/10.1016/j.matdes.2015.08.021.

[5] Fan M, Yu W, Wang W, Guo X, Jin K, Miao R, et al. Microstructure and mechanical properties of thin-multilayer Ti/Al laminates prepared by one-step explosive bonding. J Mater Eng Perform 2017;26:277–84. https://doi.org/10.1007/s11665-016-2410-z.

[6] Wang H, Wang Y. High-velocity impact welding process: a review. Metals 2019;9:144. https://doi.org/10.3390/met9020144.

[7] Chen X, Inao D, Tanaka S, Mori A, Li X, Hokamoto K. Explosive welding of Al alloys and high strength duplex stainless steel by controlling energetic conditions. J Manuf Process 2020;58:1318–33. https://doi.org/10.1016/j.jmapro.2020.09.037.

[8] Lee T, Zhang S, Vivek A, Kinsey B, Daehn G. Flyer thickness effect in the impact welding of aluminum to steel. J Manuf Sci Eng 2018;140:1–7. https://doi.org/10.1115/1.4041247.

[9] Khaustov SV, Pai VV, Lukyanov YL, Lysak VI, Kuz'min SV. Thermal effect of explosive detonation products on a flyer plate in the explosive welding of metals. Int J Heat Mass Tran 2020;163:120469. https://doi.org/10.1016/j.ijheatmasstransfer.2020.120469.

[10] Carvalho GHSFL, Galvão I, Mendes R, Leal RM, Loureiro A. Explosive welding of aluminium to stainless steel. J Mater Process Technol 2018;262:340–9. https://doi.org/10.1016/j.jmatprotec.2018.06.042.

[11] Carvalho GHSFL, Galvão I, Mendes R, Leal RM, Loureiro A. Formation of intermetallic structures at the interface of steel-to-aluminium explosive welds. Mater Char 2018;142:432–42. https://doi.org/10.1016/j.matchar.2018.06.005.

[12] Carvalho GHSFL, Galvão I, Mendes R, Leal RM, Loureiro A. Microstructure and mechanical behaviour of aluminium-carbon steel and aluminium-stainless steel clads produced with an aluminium interlayer. Mater Char 2019;155:109819. https://doi.org/10.1016/j.matchar.2019.109819.

[13] Carvalho GHSFL, Galvão I, Mendes R, Leal RM, Loureiro A. Aluminum-to-steel cladding by explosive welding. Metals 2020;10:1–18. https://doi.org/10.3390/met10081062.

[14] Loureiro A, Carvalho GHSFL, Galvão I, Leal RM, Mendes R. Explosive welding. In: Da Silva L, El-Zein M, Martins P, editors. Advanced joining processes. Elsevier; 2021. p. 207–37. https://doi.org/10.1016/B978-0-12-820787-1.00006-1.

[15] Corigliano P, Crupi V, Guglielmino E, Mariano Sili A. Full-field analysis of AL/FE explosive welded joints for shipbuilding applications. Mar Struct 2018;57:207–18. https://doi.org/10.1016/j.marstruc.2017.10.004.

[16] Carvalho GHSFL, Galvão I, Mendes R, Leal RM, Loureiro A. Friction stir welding and explosive welding of aluminum/copper: process analysis. Mater Manuf Process 2019;34:1243–50. https://doi.org/10.1080/10426914.2019.1644452.

[17] Carvalho GHSFL, Galvão I, Mendes R, Leal RM, Loureiro A. Influence of base material properties on copper and aluminium–copper explosive welds. Sci Technol Weld Join 2018;23:501–7. https://doi.org/10.1080/13621718.2017.1417783.

[18] Wei Y, Li H, Sun F, Zou J. The interfacial characterization and performance of Cu/Al-conductive heads processed by explosion welding, cold pressure welding, and solid-liquid casting. Metals 2019;9:237. https://doi.org/10.3390/met9020237.

[19] Carvalho GHSFL, Galvão I, Mendes R, Leal RM, Loureiro A. Explosive welding of aluminium to stainless steel using carbon steel and niobium interlayers. J Mater Process Technol 2020;283:116707. https://doi.org/10.1016/j.jmatprotec.2020.116707.

[20] Wilson dhileep kumar C, Saravanan S, Raghukandan K. Numerical and experimental investigation on aluminum 6061-V-grooved stainless steel 304 explosive cladding. Def. Technol. 2022;18:249–60. https://doi.org/10.1016/j.dt.2020.11.010.

[21] Liu Y, Li C, Hu X, Yin C, Liu T. Explosive welding of copper to high nitrogen austenitic stainless steel. Metals 2019;9:339. https://doi.org/10.3390/met9030339.

[22] Wang P, Chen J, Li Q, Liu D, Huang P, Jin F, et al. Study on the microstructure and properties evolution of CuCrZr/316LN-IG explosion bonding for ITER first wall components. Fusion Eng Des 2017;124:1135–9. https://doi.org/10.1016/j.fusengdes.2017.02.030.

[23] Yang M, Ma H, Shen Z, Sun Y. Study on explosive welding for manufacturing meshing bonding interface of CuCrZr to 316L stainless steel. Fusion Eng Des 2019;143:106–14. https://doi.org/10.1016/j.fusengdes.2019.03.137.

[24] Mendes R, Ribeiro JB, Loureiro A. Effect of explosive characteristics on the explosive welding of stainless steel to carbon steel in cylindrical configuration. Mater Des 2013;51:182–92. https://doi.org/10.1016/j.matdes.2013.03.069.

[25] Fang Z, Shi C, Shi H, Sun Z. Influence of explosive ratio on morphological and structural properties of Ti/Al clads. Metals 2019;9:119. https://doi.org/10.3390/met9020119.

[26] Mahmood Y, Dai K, Chen P, Zhou Q, Bhatti AA, Arab A. Experimental and numerical study on microstructure and mechanical properties of Ti-6Al-4V/Al-1060 explosive welding. Metals 2019;9:1189. https://doi.org/10.3390/met9111189.

[27] Inao D, Mori A, Tanaka S, Hokamoto K. Explosive welding of thin aluminum plate onto magnesium alloy plate using a gelatin layer as a pressure-transmitting medium. Metals 2020;10:106. https://doi.org/10.3390/met10010106.

[28] Cui Y, Liu D, Zhang Y, Deng G, Fan M, Chen D, et al. The microstructure and mechanical properties of TA1-low alloy steel composite plate manufactured by explosive welding. Metals 2020;10:663. https://doi.org/10.3390/met10050663.

[29] Rozumek D, Kwiatkowski G. The influence of heat treatment parameters on the cracks growth under cyclic bending in st-Ti clad obtained by explosive welding. Metals 2019;9:338. https://doi.org/10.3390/met9030338.

[30] Bi Z, Li X, Yang K, Kai R, Wang Q, Xu M, et al. Experimental and numerical studies of titanium foil/steel explosively welded clad plate. Def. Technol. 2022. https://doi.org/10.1016/j.dt.2022.05.001.

[31] Aceves SM, Espinosa-Loza F, Elmer JW, Huber R. Comparison of Cu, Ti and Ta interlayer explosively fabricated aluminum to stainless steel transition joints for cryogenic pressurized hydrogen storage. Int J Hydrogen Energy 2015;40:1490–503. https://doi.org/10.1016/j.ijhydene.2014.11.038.

[32] Manikandan P, Hokamoto K, Deribas AA, Raghukandan K, Tomoshige R. Explosive welding of titanium/stainless steel by controlling energetic conditions. Mater Trans 2006;47:2049–55. https://doi.org/10.2320/matertrans.47.2049.

[33] Mahmood Y, Chen P, Bataev IA, Gao X. Experimental and numerical investigations of interface properties of Ti6Al4V/CP-Ti/Copper composite plate prepared by explosive welding. Def. Technol. 2021;17:1592–601. https://doi.org/10.1016/j.dt.2020.09.003.

[34] Parchuri P, Kotegawa S, Yamamoto H, Ito K, Mori A, Hokamoto K. Benefits of intermediate-layer formation at the interface of Nb/Cu and Ta/Cu explosive clads. Mater Des 2019;166:107610. https://doi.org/10.1016/j.matdes.2019.107610.

[35] Malakhov AY, Saikov IV, Pervukhina OL, Pervukhin LB. Explosive cladding of the inner side of a steel tube with a heat-resistant niobium alloy. Inorg Mater: Applied Research 2016;7:300–2. https://doi.org/10.1134/S2075113316020131.

[36] Greenberg BA, Ivanov MA, Rybin VV, Elkina OA, Antonova OV, Patselov AM, et al. The problem of intermixing of metals possessing no mutual solubility upon explosion welding (Cu–Ta, Fe–Ag, Al–Ta). Mater Char 2013;75:51–62. https://doi.org/10.1016/j.matchar.2012.10.011.

[37] Greenberg BA, Ivanov MA, Inozemtsev AV, Pushkin MS, Patselov AM, Besshaposhnikov YR. Comparative characterisation of interfaces for two- and multi-layered Cu-Ta explosively welded composites. Compos Interfac 2020;27:705–15. https://doi.org/10.1080/09276440.2019.1690352.

[38] Yang M, Ma H, Shen Z, Huang Z, Tian Q, Tian J. Dissimilar material welding of tantalum foil and Q235 steel plate using improved explosive welding technique. Mater Des 2020;186:108348. https://doi.org/10.1016/j.matdes.2019.108348.

[39] Parchuri PK, Kotegawa S, Ito K, Yamamoto H, Mori A, Tanaka S, et al. Cladding of a crack-free W plate on Cu plates using explosive welding at higher collision velocity with lower collision angle. Result. Mater. 2020;5:100023. https://doi.org/10.1016/j.rinma.2019.100023.

[40] Baoxiang R, Gang T, Peng W, Changxing D. Study on weldability window and interface morphology of steel tube and tungsten alloy rod welded by explosive welding. Int J Refract Metals Hard Mater 2019;84:105005. https://doi.org/10.1016/j.ijrmhm.2019.105005.

[41] Bataev IA, Lazurenko DV, Tanaka S, Hokamoto K, Bataev AA, Guo Y, et al. High cooling rates and metastable phases at the interfaces of explosively welded materials. Acta Mater 2017;135:277–89. https://doi.org/10.1016/j.actamat.2017.06.038.

[42] Saravanan S, Raghukandan K. Effect of silicon carbide and wire-mesh reinforcements in dissimilar grade aluminium explosive clad composites. Def. Technol. 2020;16:1160–6. https://doi.org/10.1016/j.dt.2019.12.009.

[43] Saravanan S, Inokawa H, Tomoshige R, Raghukandan K. Microstructural characterization of silicon carbide reinforced dissimilar grade aluminium explosive clads. Def. Technol. 2020;16:689–94. https://doi.org/10.1016/j.dt.2019.10.008.

[44] Mendes R, Ribeiro J, Plaksin I, Campos J, Tavares B. Differences between the detonation behavior of emulsion explosives sensitized with glass or with polymeric micro-balloons. J Phys Conf 2014;500:1–6. https://doi.org/10.1088/1742-6596/500/5/052030.

[45] Hoseini Athar MM, Tolaminejad B. Weldability window and the effect of interface morphology on the properties of Al/Cu/Al laminated composites

fabricated by explosive welding. Mater Des 2015;86:516–25. https://doi.org/10.1016/j.matdes.2015.07.114.
[46] Leitão C, Galvão I, Leal RM, Rodrigues DM. Determination of local constitutive properties of aluminium friction stir welds using digital image correlation. Mater Des 2012;33:69–74. https://doi.org/10.1016/j.matdes.2011.07.009.
[47] Kennedy JE. Gurney energy of explosives: estimation of the velocity and impulse imparted to driven metal. New Mexico, USA: Sandia Laboratories; 1970.
[48] El-Sobky H. Mechanics of explosive welding. In: Blazynski TZ, editor. Explosive welding, forming and compaction. Dordrecht: Springer Netherlands; 1983. p. 189–217. https://doi.org/10.1007/978-94-011-9751-9_6.
[49] Patterson RA. Fundamentals of explosion welding. ASM handbook - volume 6: welding, brazing and soldering. Materials Park, Ohio, USA: ASM International; 1993. p. 160–4. https://doi.org/10.31399/asm.hb.v06.a0001351.
[50] Cooper PW. Explosive engineering. New York, USA: Wiley-VCH; 1996.
[51] Carvalho GHSFL, Mendes R, Leal RM, Galvão I, Loureiro A. Effect of the flyer material on the interface phenomena in aluminium and copper explosive welds. Mater Des 2017;122:172–83. https://doi.org/10.1016/j.matdes.2017.02.087.
[52] Ribeiro JB, Mendes R, Loureiro A. Review of the weldability window concept and equations for explosive welding. J Phys Conf 2014;500:052038. https://doi.org/10.1088/1742-6596/500/5/052038.
[53] Deribas AA, Zakharenko ID. Surface effects with oblique collisions between metallic plates. Combust Explos Shock Waves 1974;10:358–67. https://doi.org/10.1007/BF01463767.
[54] Carpenter SH, Wittman RH. Explosion welding. Annu Rev Mater Sci 1975;5:177–99. https://doi.org/10.1146/annurev.ms.05.080175.001141.
[55] Rosset WS. Analysis of explosive bonding parameters. Mater Manuf Process 2006;21:634–8. https://doi.org/10.1080/10426910600611136.
[56] Cowan GR, Bergmann OR, Holtzman AH. Mechanism of bond zone wave formation in explosion-clad metals. Metall Mater Trans B 1971;2:3145–55. https://doi.org/10.1007/BF02814967.
[57] Grignon F, Benson D, Vecchio KS, Meyers MA. Explosive welding of aluminum to aluminum: analysis, computations and experiments. Int J Impact Eng 2004;30:1333–51. https://doi.org/10.1016/j.ijimpeng.2003.09.049.
[58] Gülenç B, Kaya Y, Durgutlu A, Gülenç İT, Yıldırım MS, Kahraman N. Production of wire reinforced composite materials through explosive welding. Arch Civ Mech Eng 2016;16:1–8. https://doi.org/10.1016/j.acme.2015.09.006.
[59] Li X, Ma H, Shen Z. Research on explosive welding of aluminum alloy to steel with dovetail grooves. Mater Des 2015;87:815–24. https://doi.org/10.1016/j.matdes.2015.08.085.
[60] Aizawa Y, Nishiwaki J, Harada Y, Muraishi S, Kumai S. Experimental and numerical analysis of the formation behavior of intermediate layers at explosive welded Al/Fe joint interfaces. J Manuf Process 2016;24:100–6. https://doi.org/10.1016/j.jmapro.2016.08.002.
[61] Gale WF, Totemeir TC. General physical properties. In: Gale WF, Totemeir TC, editors. Smithells metals reference book. eighth ed. Oxford, England: Elsevier; 2004. p. 14. https://doi.org/10.1016/B978-075067509-3/50017-8. 1-14–45.
[62] Livne Z, Munitz A. Characterization of explosively bonded iron and copper plates. J Mater Sci 1987;22:1495–500. https://doi.org/10.1007/BF01233153.
[63] Zhang H, Jiao KX, Zhang JL, Liu J. Experimental and numerical investigations of interface characteristics of copper/steel composite prepared by explosive welding. Mater Des 2018;154:140–52. https://doi.org/10.1016/j.matdes.2018.05.027.
[64] Zhang H, Jiao KX, Zhang JL, Liu J. Comparisons of the microstructures and micro-mechanical properties of copper/steel explosive-bonded wave interfaces. Mater Sci Eng 2019;756:430–41. https://doi.org/10.1016/j.msea.2019.04.064.
[65] Zhang H, Jiao KX, Zhang JL, Liu J. Microstructure and mechanical properties investigations of copper-steel composite fabricated by explosive welding. Mater Sci Eng 2018;731:278–87. https://doi.org/10.1016/j.msea.2018.06.051.
[66] Carvalho GHSFL, Galvão I, Mendes R, Leal RM, Loureiro A. Weldability of aluminium-copper in explosive welding. Int J Adv Manuf Technol 2019;103:3211–21. https://doi.org/10.1007/s00170-019-03841-9.
[67] Durgutlu A, Gülenç B, Findik F. Examination of copper/stainless steel joints formed by explosive welding. Mater Des 2005;26:497–507. https://doi.org/10.1016/j.matdes.2004.07.021.
[68] Kahraman N, Gülenç B. Microstructural and mechanical properties of Cu-Ti plates bonded through explosive welding process. J Mater Process Technol 2005;169:67–71. https://doi.org/10.1016/j.jmatprotec.2005.02.264.
[69] Gülenç B. Investigation of interface properties and weldability of aluminum and copper plates by explosive welding method. Mater Des 2008;29:275–8. https://doi.org/10.1016/j.matdes.2006.11.001.
[70] Zamani E, Liaghat GH. Explosive welding of stainless steel–carbon steel coaxial pipes. J Mater Sci 2012;47:685–95. https://doi.org/10.1007/s10853-011-5841-9.
[71] Durgutlu A, Okuyucu H, Gülenç B. Investigation of effect of the stand-off distance on interface characteristics of explosively welded copper and stainless steel. Mater Des 2008;29:1480–4. https://doi.org/10.1016/j.matdes.2007.07.012.
[72] Prümmer R. The use of lead in explosive cladding. Propellants, Explos Pyrotech 1976;1:103–7. https://doi.org/10.1002/prep.19760010506.
[73] Hokamoto K, Izuma T, Fujita M. New explosive welding technique to weld aluminum alloy and stainless steel plates using a stainless steel intermediate plate. Metall Trans A 1993;24:2289–97. https://doi.org/10.1007/BF02648602.
[74] Hokamoto K, Chiba A, Fujita M, Izuma T. Single-shot explosive welding technique for the fabrication of multilayered metal base composites: effect of welding parameters leading to optimum bonding condition. Compos Eng 1995;5:1069–79. https://doi.org/10.1016/0961-9526(95)00059-V.
[75] Carpenter SH. Chapter 53 explosion welding: a review. In: Meyers MA, Murr LE, editors. Shock waves and high-strain-rate phenomena in metals. first ed. Springer US; 1981. p. 941–59.
[76] Paul H, Lityńska-Dobrzyńska L, Prazmowski M. Microstructure and phase constitution near the interface of explosively welded aluminum/copper plates. Metall Mater Trans 2013;44:3836–51. https://doi.org/10.1007/s11661-013-1703-1.
[77] Paul H, Morgiel J, Baudin T, Brisset F, Prazmowski M, Miszczyk M. Characterization of explosive weld joints by TEM and SEM/EBSD. Arch Metall Mater 2014;59:1129–36. https://doi.org/10.2478/amm-2014-0197.
[78] Bataev IA, Tanaka S, Zhou Q, Lazurenko DV, Junior AMJ, Bataev AA, et al. Towards better understanding of explosive welding by combination of numerical simulation and experimental study. Mater Des 2019;169:107649. https://doi.org/10.1016/j.matdes.2019.107649.
[79] Khaustov SV, Kuz'min SV, Lysak VI, Pai VV. Thermal processes in explosive welding. Combust Explos Shock Waves 2014;50:732–8. https://doi.org/10.1134/S0010508214060161.
[80] Grady D. Shocks and structured waves. Physics of shock and impactume 1. IOP Publishing Ltd; 2017. https://doi.org/10.1088/978-0-7503-1254-7ch1. 1.1-1.103.
[81] Manikandan P, Lee JO, Mizumachi K, Mori A, Raghukandan K, Hokamoto K. Underwater explosive welding of thin tungsten foils and copper. J Nucl Mater 2011;418:281–5. https://doi.org/10.1016/j.jnucmat.2011.07.013.
[82] Paul H, Miszczyk MM, Chulist R, Prażmowski M, Morgiel J, Gałka A, et al. Microstructure and phase constitution in the bonding zone of explosively welded tantalum and stainless steel sheets. Mater Des 2018;153:177–89. https://doi.org/10.1016/j.matdes.2018.05.014.
[83] Handbook ASM. Volume 3 - alloy phase diagrams. tenth ed. Materials Park, Ohio, USA: ASM International; 1992.
[84] Fronczek DM, Chulist R, Litynska-Dobrzynska L, Lopez GA, Wierzbicka-Miernik A, Schell N, et al. Microstructural and phase composition differences across the interfaces in Al/Ti/Al explosively welded clads. Metall Mater Trans 2017;48:4154–65. https://doi.org/10.1007/s11661-017-4169-8.
[85] Fronczek DM, Wojewoda-Budka J, Chulist R, Sypien A, Korneva A, Szulc Z, et al. Structural properties of Ti/Al clads manufactured by explosive welding and annealing. Mater Des 2016;91:80–9. https://doi.org/10.1016/j.matdes.2015.11.087.
[86] Linse VD, Temple PI. Explosion welding. AWS welding handbook – volume 2 - welding processes. eighth ed. USA: American Welding Society; 1991. p. 765–81.